Seasonal evolution of the intraseasonal variability of China summer precipitation

Article *in* Climate Dynamics · April 2020

DOI: 10.1007/s00382-020-05251-0

6 authors, including:

Fei Liu
Sun Yat-Sen University
54 PUBLICATIONS **761** CITATIONS
SEE PROFILE

Ouyang Yu
Nanjing University of Information Science & Technology
2 PUBLICATIONS **0** CITATIONS
SEE PROFILE

Bin Wang
University of Hawai'i at Mānoa
124 PUBLICATIONS **6,104** CITATIONS
SEE PROFILE

Jing Yang
Beijing Normal University
63 PUBLICATIONS **1,586** CITATIONS
SEE PROFILE

Climate Dynamics
https://doi.org/10.1007/s00382-020-05251-0

Seasonal evolution of the intraseasonal variability of China summer precipitation

Fei Liu[1,2,3] · Yu Ouyang[3] · Bin Wang[4] · Jing Yang[5] · Jian Ling[6] · Pang-Chi Hsu[3]

Received: 10 November 2019 / Accepted: 15 April 2020

Abstract
Seasonal cycle of China summer precipitation has significant impacts on its subseasonal predictability; yet current understanding of seasonal evolution of the intraseasonal variability (ISV) remains limited. Here, we show that the ISV of China summer precipitation features a distinct three-stage evolution during early summer, Meiyu season, and late summer. There are two common leading ISV modes: a uniform mode (UM) over southeastern China and a dipole mode (DM) between coastal southeastern China and mid-lower reaches of the Yangtze River Basin, which occur during all three stages with a dominant period of 8–15 days in the early and late summers and 8–25 days during Meiyu season. These two modes show southward propagation in early summer, but they are independent from each other in the other two stages. In early summer, both UM and DM are only related to mid-latitude wave train, and no preceding signal is found in the tropics due to the weak western North Pacific (WNP) monsoon trough. In contrast, during the Meiyu season and late summer, preceding tropical signals are observed when the WNP monsoon trough becomes strong. In the late summer, the effect of mid-latitude wave train is weak as the westerly jet-induced wave guide is far away from southeastern China. An improved subseasonal prediction system is expected to be benefited from consideration of the seasonal evolution of China summer precipitation ISV.

Keywords Intraseasonal variability · China summer precipitation · Meiyu season · Seasonal evolution

1 Introduction

Intraseasonal variability (ISV) is the dominant source of subseasonal climate predictability (Vitart et al. 2017). The recent improvement of subseasonal prediction of western United States precipitation and temperature may be partly attributed to the inclusion of seasonal cycle (Hwang et al. 2019), which indicates that the information about seasonal change of the ISV should be considered for a skillful subseasonal prediction. Thus, we investigate whether the regional ISV has significant seasonal evolution or not here.

China, with the largest population in the world, is influenced by one of the strongest summer monsoon systems; and the monsoon variability has large impacts on its climate and weather, such as floods, droughts, and other climate extremes, and its living environments (Chen et al. 2006; Tao and Chen 1987; Wang 2006). Investigating China summer precipitation ISV is important for subseasonal prediction and associated water resource safety and disaster reduction.

Located between the tropics and mid latitude, the ISV in China is affected by both tropical and extratropical circulation anomalies (Stan et al. 2017), such as tropical

✉ Fei Liu
liuf@nuist.edu.cn

1 School of Atmospheric Sciences, and Guangdong Province Key Laboratory for Climate Change and Natural Disaster Studies, Sun Yat-sen University, Zhuhai 519082, China

2 Southern Marine Science and Engineering Guangdong Laboratory (Zhuhai), Zhuhai 519082, China

3 Earth System Modeling and Climate Dynamics Research Center, Nanjing University of Information Science and Technology, Nanjing 210044, China

4 Department of Atmospheric Sciences and International Pacific Research Center, University of Hawaii at Manoa, Honolulu, HI 96822, USA

5 State Key Laboratory of Earth Surface Processes and Resource Ecology, Beijing Normal University, Beijing 100875, China

6 Institute of Atmospheric Sciences, Chinese Academy of Sciences, Beijing 10029, China

Published online: 21 April 2020

boreal-summer intraseasonal oscillation (Chen and Zhu 2001; Liang and Ding 2012; Mao and Chan 2005; Zhu and Xu 2000), quasi-biweekly oscillation (Hsu et al. 2016; Wei et al. 2017; Yang et al. 2010), and mid-latitude wave trains (Gao et al. 2017; Yang et al. 2017).

The precipitation over the lower reaches of the Yangtze River is shown to experience significant biweekly and 21–30-day oscillation (Huang et al. 2008; Yang et al. 2010). The former is initiated by the upper-level southeastward-propagating mid-latitude wave train, while the latter is associated with the low-to-mid level eastward-westward oscillation of the western North Pacific (WNP) subtropical high (Yang et al. 2010). A large amount of the extreme events over the Yangtze River Basin (YRB) are attributed to ISV over the basin. The probability of extreme rainfall over the Yangtze River and South China regions is increased by about 40% during the wet phase of the second boreal-summer intraseasonal oscillation mode (Ren et al. 2018). And nearly 55% heat wave events in July and August over the YRB is found to be related to the low-level anticyclonic anomaly caused by both mid-latitude and tropical wave trains (Gao et al. 2017).

Precipitation over southeastern China has significant oscillation of 12–30 days, which has the largest amplitude during June (Wei et al. 2017). The wet phase of ISV over southeastern China is induced by subtropical low-level WNP anticyclone anomaly and by upper-tropospheric anticyclone anomaly over northeastern China (Cao et al. 2012). The probability of extreme rainfall over southeastern China is found to be increased by about 35–45% at the wet phase of the first boreal summer intraseasonal oscillation mode (Ren et al. 2018).

The summer precipitation over the Tibetan Plateau also exhibits a dominant quasi-biweekly variability, which is found to be related to the southeastward propagating non-stationary wave train originated from the summertime Arctic Oscillation (Wang et al. 2018) and the northwestward/northward migration of low-level tropical wave train (Yang et al. 2017). These studies on ISV of China summer precipitation, however, focused on different regions with different dominant modes. It is still unclear what the dominant mode of ISV is for the whole China summer precipitation.

The East Asian summer monsoon (EASM) usually displays distinct stepwise northward and northeastward advances (Lau and Waliser 2005; Wu and Wang 2001), with two abrupt northward jumps and three stationary periods, such as the pre-summer rainy season in South China from early- to mid-May, Meiyu/Baiu rainy season in the YRB and Japan from late-May to mid-July; and it finally penetrates to North China, Korea, and the topical western Pacific from late-July to early-August (Chen 2004; Ding 2004; Ding and Chan 2005; Son et al. 2019). The EASM advances were usually found to be related to the phase transition of climatological intraseasonal oscillation (Ding and Wang 2008; Wang and LinHo 2002; Wang et al. 2004; Wang and Xu 1997).

Due to the advance of the EASM, the seasonal evolution of ISV of China summer precipitation needs to be investigated. The changes in spatial distribution and propagating path of 12–20-day variability over East Asia between early and late summers were attributed to the abrupt change of the mean state, including the northward migration of westerly jet, South Asian high, and WNP subtropical high (Yang et al. 2014). The quasi-biweekly oscillation over the South China Sea was found to be originated from eastern Japan during early summer, and from the east of the Philippines during late summer (Wang et al. 2015). For the dominant mode of ISV of whole China summer precipitation, it is not clear whether significant seasonal evolution exists or not, and if it does, what the underlying mechanism is.

In this paper, we study the seasonal evolution of ISV of China summer precipitation and explore its underlying mechanism. We will also focus on potential predictability source in different stages of the seasonal evolution. The paper is organized as follows. In Sect. 2, we describe data and methods. Seasonal evolution of ISV activity is presented in Sect. 3. Leading modes of ISV in different stages are discussed in Sect. 4. We investigate potential predictability for the ISV in different stages in Sect. 5. Conclusions and discussion are given in Sect. 6.

2 Data and methods

We use gridded daily precipitation over China from the newly released CN05.1 dataset by China's National Climate Center (Wu and Gao 2013; Xu et al. 2009). It is interpolated to a high resolution of 0.25° using data from 2400 stations. The climatological mean is obtained using thin-plate smoothing spline interpolation (Hutchinson 1995), and its anomaly, using angular distance weighting method (New et al. 2000; Shepard 1984). Daily precipitation from the Climate Prediction Center (CPC) Global Precipitation data with a resolution of $0.5° \times 0.5°$, provided by the National Oceanic and Atmospheric Administration (NOAA) (Xie et al. 2007), is also used.

Daily outgoing longwave radiation (OLR) dataset at $2.5° \times 2.5°$ resolution from the NOAA (Liebmann and Smith 1996) is used, which is a good proxy for organized deep convection in the tropics on the intraseasonal time scale (Kikuchi et al. 2011; Lee et al. 2013; Wheeler and Hendon 2004). Daily wind field is obtained from the National Centers for Environmental Prediction (NCEP) Reanalysis data (Kalnay et al. 1996). The study period covers 38 years from 1979 to 2016, and the boreal summer season is defined from

1st May to 31st August. The data set of the boundary of the Tibetan Plateau is from Zhang et al. (2002).

Since precipitation in China is affected by tropical 8–25-day oscillation, 30–60-day intraseasonal oscillation, and mid-latitude quasi-biweekly variability, we perform 8–80-day butterworth bandpass filtering (Duchon 1979) to isolate the intraseasonal signals, which include both 8–25 and 30–50 day oscillations. Similar results were also obtained based on the intraseasonal signal after using 5-day running mean and removing the first three harmonics of the annual cycle (not shown).

For each day, the ISV activity is calculated as 31-day-averaged variance of intraseasonal signal with 15 days before and after the selected day. Since the leading ISV modes of China summer precipitation have a significant period of 8–25 days rather than 30–60 days, which will be shown later, we use 31-day average to calculate the ISV activity. Sixty-one-day average is also used, and similar results are obtained (not shown). We calculate the ISV variance for each year, and then average them over the 38 years as the climatological ISV activity for each calendar day. To identify the major modes of seasonal evolution of the ISV activity, we perform EOF analysis on the climatological ISV activity. We also perform EOF analysis on the intraseasonal China summer precipitation to obtain the leading modes of the ISV. Each Principle Component (PC) is normalized by its standard deviation, and the EOF is scaled by multiplying this standard deviation. Wavelet analysis on the PC is performed to calculate the spectrum of the ISV. Potential predictability source for these ISVs is detected by using regression maps. Since a bandpass filter is used, the effective degree of freedom (Livezey and Chen 1983) is calculated for significant test based on two-tailed Student *t* test.

To investigate possible sources and propagation routes of the mid-latitude wave train, a phase-independent wave activity flux (WAF) formulated by Takaya and Nakamura (2001) is calculated, which has been used for studying the mid-latitude wave train on the intraseasonal timescale (Gao et al. 2017; Wang et al. 2018; Yang and Li 2016). A two-dimensional horizontal WAF can be expressed as follows:

$$W = \frac{1}{2|\bar{U}|}\begin{bmatrix} \bar{u}\left(\psi_x'^2 - \psi'\psi_{xx}'\right) + \bar{v}\left(\psi_x'\psi_y' - \psi'\psi_{xy}'\right) \\ \bar{u}\left(\psi_x'\psi_y' - \psi'\psi_{xy}'\right) + \bar{v}\left(\psi_y'^2 - \psi'\psi_{yy}'\right) \end{bmatrix},$$

where u and v are the zonal and meridional components of the flow, respectively;$|U|$ is wind velocity; and ψ is the stream function. The bar and prime represent the low-frequency background state (greater than 31 days) and the ISV, respectively.

3 Seasonal evolution of ISV activity

During the boreal summer, China is controlled by the EASM with strong precipitation over its southeastern region, and the maximum summer precipitation is larger than 10 mm day^{-1} (Fig. 1a). Four strong precipitation centers are observed along the Yangtze River. From southeastern to northwestern China, the seasonal-mean precipitation decays quickly, and the average precipitation is even below 1 mm day^{-1} over some parts of northwestern China. Distribution of climatological summer ISV activity, represented by the variance of 8–80-day filtered precipitation anomaly for the whole summer, generally follows that of seasonal-mean precipitation, which has the strong ISV activity over coastal southeastern China, southwestern China, and the mid-lower reaches of the Yangtze River (Fig. 1b). The ISV in south part of Yunnan Province and eastern Tibetan Plateau is very weak, against strong seasonal-mean precipitation there. The weak ISV activity in south part of Yunnan Province and eastern Tibetan Plateau was also present in the CPC dataset (not shown).

The leading modes of seasonal evolution of ISV activity can be calculated by performing EOF analysis on the climatological 31-day-sliding variance of China intraseasonal precipitation anomaly from 1st May to 31st August. We find two significant modes that are statistically distinguishable from each other and from other higher modes according to the rule of North et al. (1982). The percentage variances accounted for by these two leading modes are

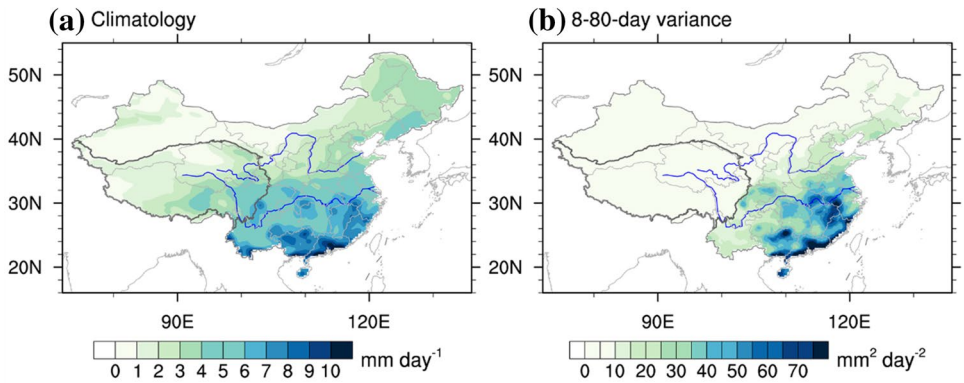

Fig. 1 Climatological summer precipitation in China and ISV activity. **a** The boreal-summer (May–August) averaged precipitation (mm day^{-1}) during 1979–2016. **b** The same as **a** except for variance (mm^2 day^{-2}) of 8–80-day filtered precipitation anomaly

50.6% and 39.6%, respectively. The first leading mode is demonstrated by strongest positive anomaly in southwestern China and south of the mid-lower reaches of the Yangtze River (Fig. 2a). The second mode has positive anomaly over whole central and eastern China including coastal southeastern China, east of the Tibetan Plateau, and northeastern China, except for negative anomaly over inland southeastern China (Fig. 2b).

Figure 2c shows the PCs of these two leading modes for the seasonal evolution of ISV activity. The first leading mode is mainly characterized by a strong positive phase around mid-June to early-July, associated with the Meiyu season. In May and August, this mode is in its negative phase. The second mode changes its phase in late-June, from negative phase around May to positive phase around August; and the strongest positive phase occurs near late-July, which means that strong ISV over the east of the Tibetan Plateau and coastal region of southeastern China only peaks around late-July.

These two leading modes for the seasonal evolution of ISV activity can also be obtained when we extend to whole Asia based on the CPC data, while the sequence of these two leading modes is exchanged compared to that of China (Figs. 2, 3). The first leading mode (Fig. 3a), related to the second mode of China's seasonal evolution of ISV activity (Fig. 2b), shows uniform positive anomalies over whole Asia except for the negative anomaly over inland southeastern China. The positive anomalies in southwestern China and south of the mid-lower reaches of the Yangtze River in late-June of the second mode, are accompanied by negative anomalies over India, Philippines and North Korea (Fig. 3b).

In summary, the positive phase of the first mode dominates the period from mid-June to mid-July, while the positive and negative phases of the second mode peak before mid-June and after mid-July, respectively (Fig. 2), which are related to the EASM rain belt jump around mid-June and mid-July, respectively (Ding 2004; Ding and Chan 2005). Thus, we classify the seasonal evolution of China precipitation ISV into three stages: early summer from 1st May to 14th June, Meiyu season from 15th June to 15th July and late summer from 16th July to 31st August.

The ISV activity of China summer precipitation exhibits different distributions in these three stages. In early summer (Fig. 4a), the ISV mainly prevails in southeastern China, with maximum activity in the coastal region of South China, north part of Guangxi Province, and north part of Fujian Province. The ISV activity becomes stronger during the Meiyu season, and the ISV also prevails in the mid-lower reaches of the Yangtze River and Jianghuai region (Fig. 4b). In late summer, the maximum ISV activity retreats to the coastal region of southeastern China and eastern Tibetan Plateau (Fig. 4c). This seasonal evolution of ISV activity follows that of mean precipitation closely, except that the weak ISV activity around south part of Yunnan Province and eastern Tibetan Plateau is against strong mean precipitation there in the Meiyu season and late summer (Fig. 4d–f).

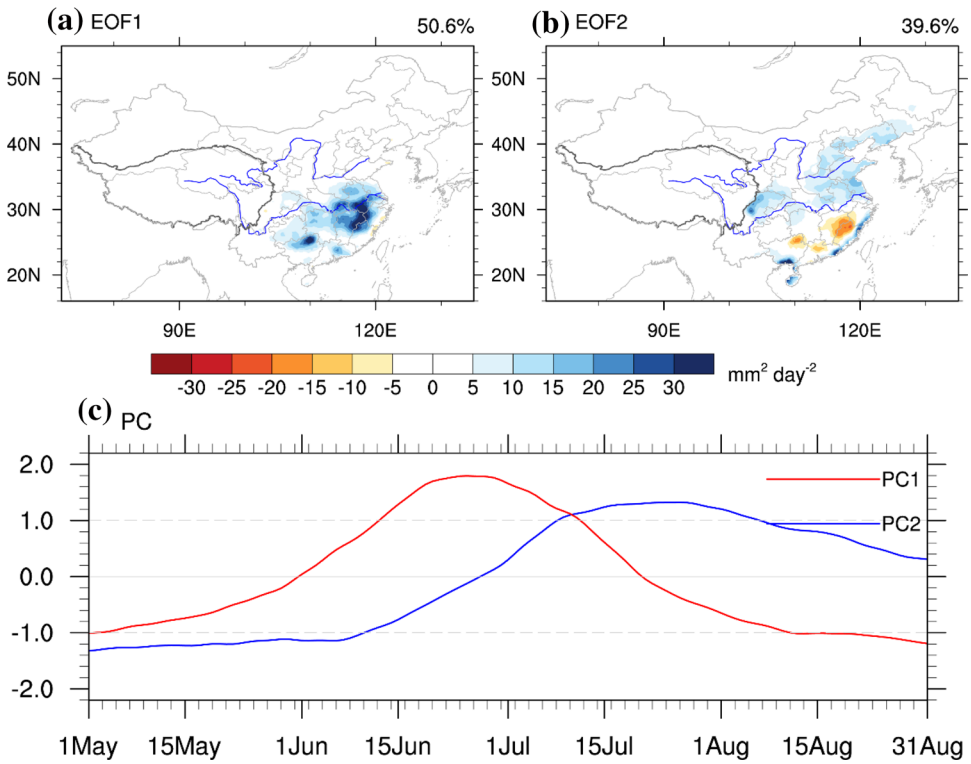

Fig. 2 Seasonal evolution of ISV activity of China summer precipitation. **a**, **b** The first and second EOF modes, respectively, of climatological 31-day-sliding variance ($mm^2\ day^{-2}$) of 8–80-day-filtered precipitation anomaly over China from 1st May to 31st August based on the CN05.1 dataset. **c** The PCs for the first (red) and second (blue) leading modes, respectively. Each time series has been normalized

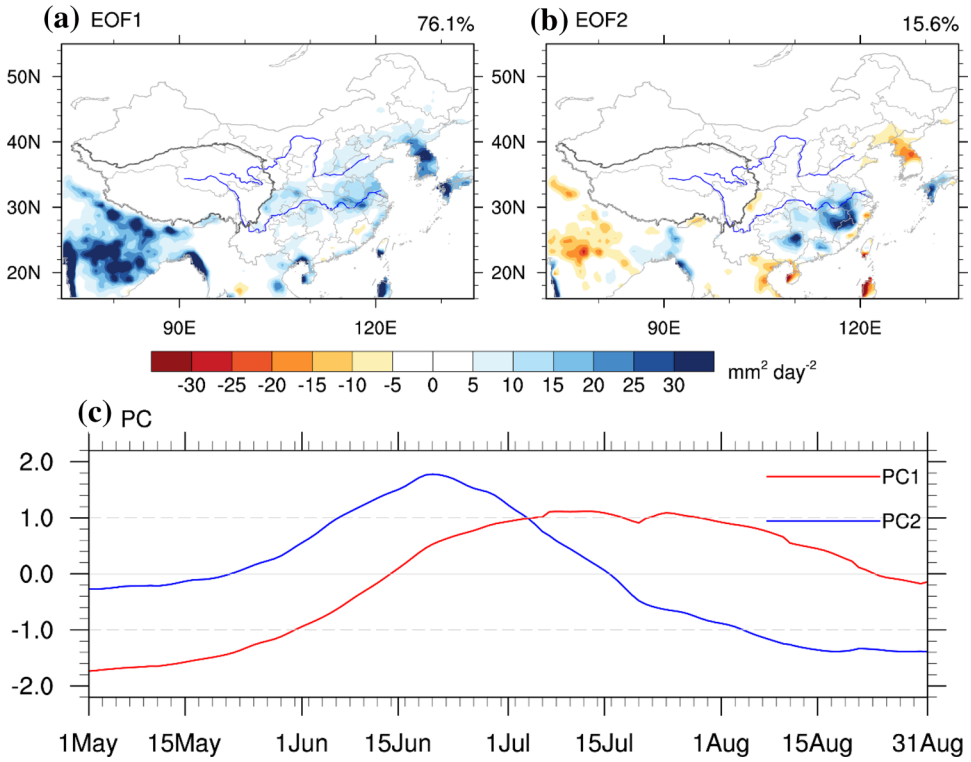

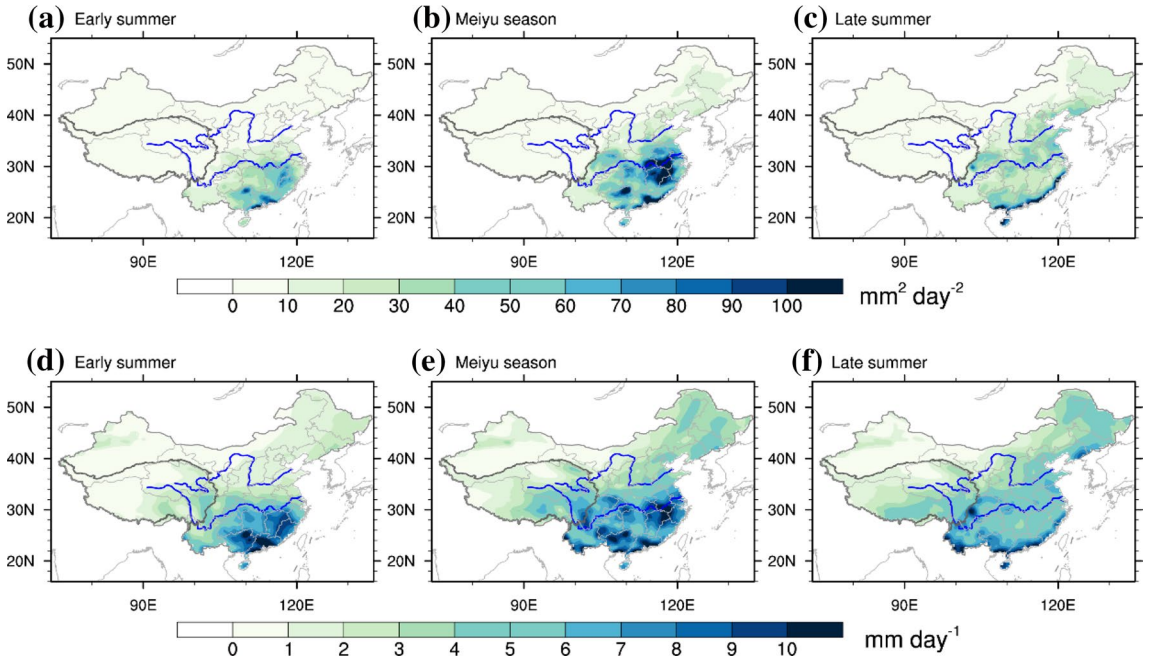

Fig. 3 Same as Fig. 2, except for the whole Asia based on the CPC data

Fig. 4 ISV activity during different stages. Variance ($mm^2\ day^{-2}$) of 8–80-day-filtered precipitation anomaly over China for **a** early summer (1st May to 14th June), **b** Meiyu season (15th June to 15th July), and **c** late summer (16th July to 31st August) from 1979 to 2016. **d**–**f** The same as **a**–**c** except for mean precipitation ($mm\ day^{-1}$) in each stage

4 ISV in different stages

The leading modes of ISV of China summer precipitation can be obtained by performing EOF analysis on the 8–80-day-filtered summer precipitation from 1979 to 2016. For the whole boreal summer, the ISV of China summer precipitation is dominated by two leading modes, which are significantly distinguishable from other higher modes. The percentage variances accounted for by these two leading modes are 14.5% and 11.2%, respectively. The first leading mode is dominated by strong uniform positive precipitation anomaly over the whole southeastern China to the south of the Yangtze River, while weak negative anomaly over the Jianghuai region (Fig. 5a). The second mode, however, is dominated by dipole precipitation anomalies with negative anomaly over the coastal region of southeastern China and positive anomaly over the mid-lower reaches of the Yangtze River (Fig. 5b).

EOF analysis is also performed on intraseasonal precipitation anomalies in early summer, Meiyu season, and late summer. The leading uniform mode (UM) and the second dipole mode (DM) are observed in each stage (Fig. 5c–h). For these two leading modes, each stage has significant pattern correlation and PC correlation with the whole summer, and their correlation coefficients are all above 0.85 ($p < 0.01$).

Since the PCs are normalized, the ISV strengths during different stages can be represented by the amplitude of EOF anomaly. In early summer, the precipitation anomaly of UM over southeastern China is stronger than those of DM over the coastal region of southeastern China and over the mid-lower reaches of the Yangtze River (Fig. 5c, d), consistent with the ISV activity distribution in Fig. 4a. The precipitation anomaly over the mid-lower reaches of the Yangtze River for DM only becomes strong during the Meiyu season (Fig. 5f). The precipitation anomaly of UM during late summer is maximum over the coastal region of southeastern China (Fig. 5g). Consistent with strong ISV activity in the Meiyu season (Fig. 4b), the precipitation anomalies of UM and DM in the Meiyu season are also stronger than those in the other two stages.

The strong precipitation anomalies of UM over southeastern China during early summer (Fig. 5c) and over the coastal region of southeastern China in late summer (Fig. 5g) are consistent with the positive and negative phase of the second mode of seasonal evolution of ISV activity (Fig. 2), respectively. The strong precipitation anomaly of DM over the mid-lower reaches of the Yangtze River (Fig. 5f), however, is related to the positive phase of the leading mode (Fig. 2).

Since the PCs from EOF analysis for the whole summer are highly correlated with those calculated from each stage, these PCs can be used as the indexes for UM and DM in each stage. The short period of less than 45 days in each stage usually removes some low-frequency intraseasonal signal; thus, we perform the wavelet analysis on the PCs from EOF analysis for the whole summer to calculate ISV spectra during different summer stages.

During early and late summers, UM and DM are dominated by 8–15-day period, while their periods extend to 8–25 days during the Meiyu season (Fig. 6). Compared to the ISV in early and late summers, the ISV during the Meiyu season is also stronger. For the whole summer, both UM and DM have a significant period from 8 to 25 days; and they peak at 11 days and 12 days, respectively, consistent with previous work on regional precipitation anomaly of the lower reaches of the Yangtze River (Huang et al. 2008; Yang et al. 2010), southeastern China (Wei et al. 2017), and eastern Tibetan Plateau (Yang et al. 2017).

To explore the relationship between these two leading modes, the 31-day-sliding lead-lag correlation between PC1 and PC2 for the whole summer is shown (Fig. 7a). Significant correlation is only observed in early summer, and PC2 tends to lead PC1 by about 2–3 days, which means that the positive precipitation anomaly over the mid-lower reaches of the Yangtze River will move to southeastern China in 2–3 days in early summer. The maximum correlation coefficient, however, is only 0.3, which is much smaller than that (0.56) between Real-time Multivariate Madden-Julian Oscillation series 1 and 2 (Wheeler and Hendon 2004) and than that (about 0.45) between PC3 and PC4 of boreal-summer intraseasonal oscillation index (Lee et al. 2013). In the Meiyu season and late summer, the relationship between UM and DM is insignificant, which means these two leading modes are independent from each other. Similar results are also obtained for the PC in each stage (Fig. 7b).

5 Potential ISV predictability in different stages

Since ISV over China is affected by both tropical and mid-latitude systems (Stan et al. 2017), we detect tropical convection system by using regressed OLR anomaly and detect mid-latitude wave train by using regressed upper-tropospheric wind anomaly and WAF. The significant preceding signal in the tropics and mid latitude can be used as potential predictability source for these two leading modes of ISV of China summer precipitation.

5.1 Early summer

During early summer, positive OLR anomaly or dry convection anomaly propagate southward from southeastern China at day −6 to the South China Sea and Philippine

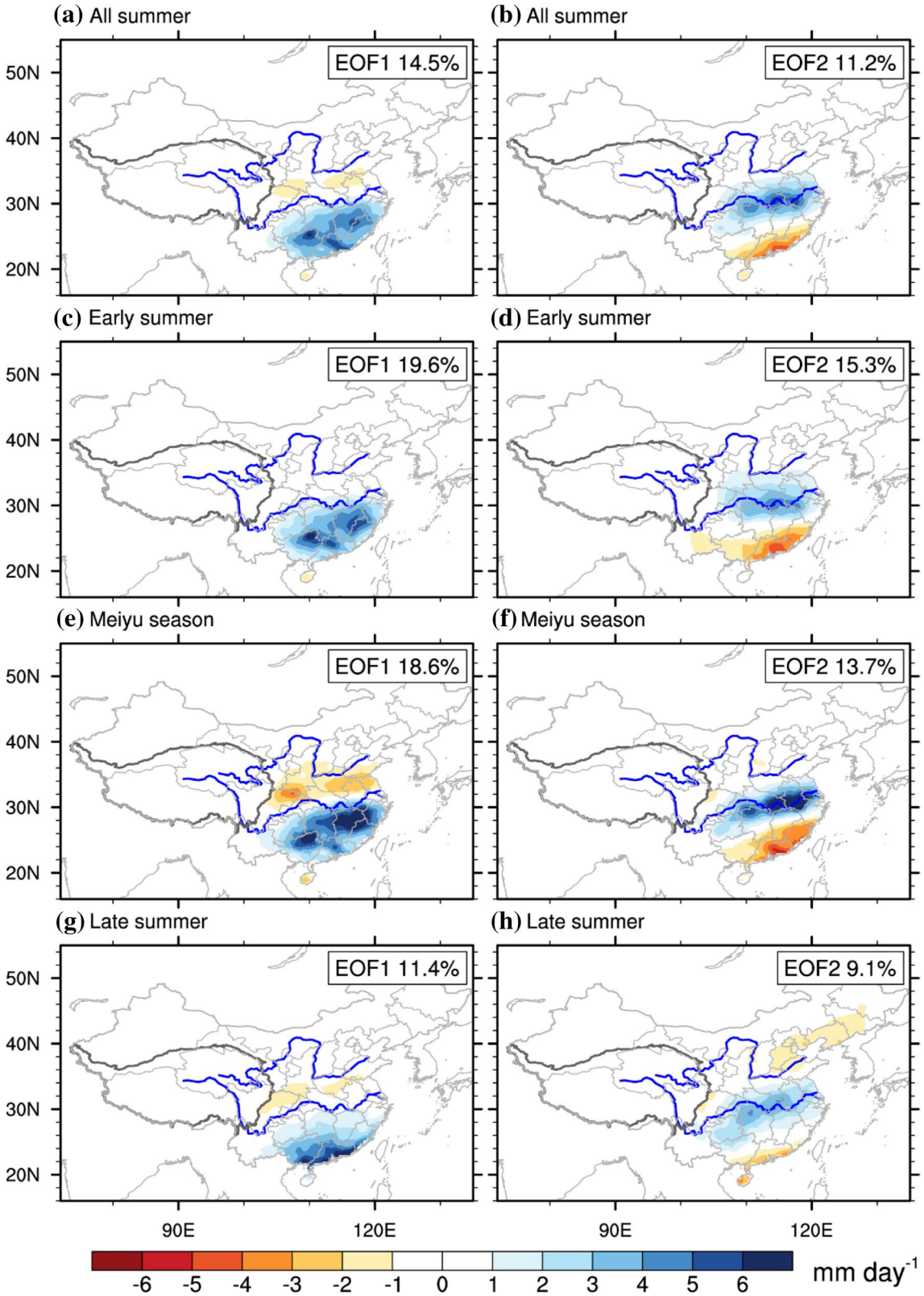

Fig. 5 Dominant ISV modes during different stages. **a**, **b** The first and second EOF modes, respectively, of 8–80-day-filtered precipitation anomaly (mm day^{-1}) over China from 1st May to 31st August during 1979–2016. **c**–**d**, **e**–**f**, and **g**–**h** are the same as **a**–**b** except for early summer, Meiyu season, and late summer, respectively

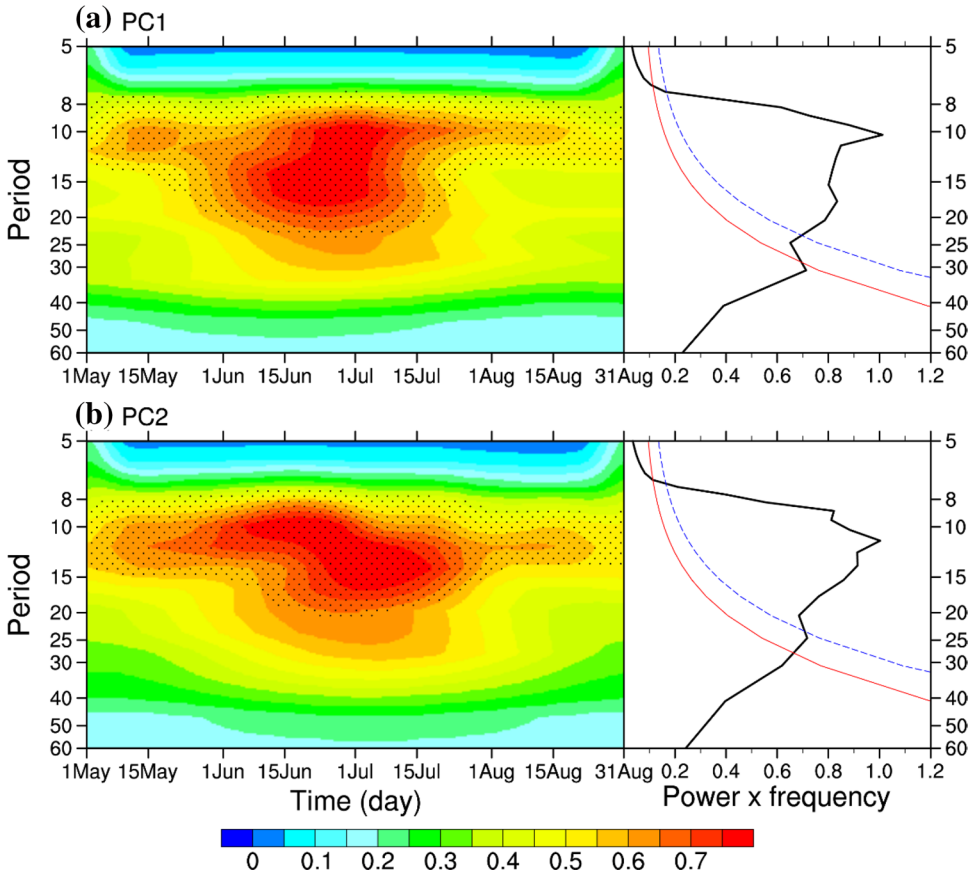

Fig. 6 Seasonal evolution of ISV period of China summer precipitation. **a** The square root of wavelet spectrum (left panel), multiplied by frequency, of the PC of leading EOF of Fig. 5a, calculated using the whole summer time series. Stippling denotes spectrum significant at the 95% confidence level. Also shown is the average of the summer (right panel); and red and dashed lines denote the red noise and 95% confidence level, respectively. **b** The same as **a** except for the second EOF

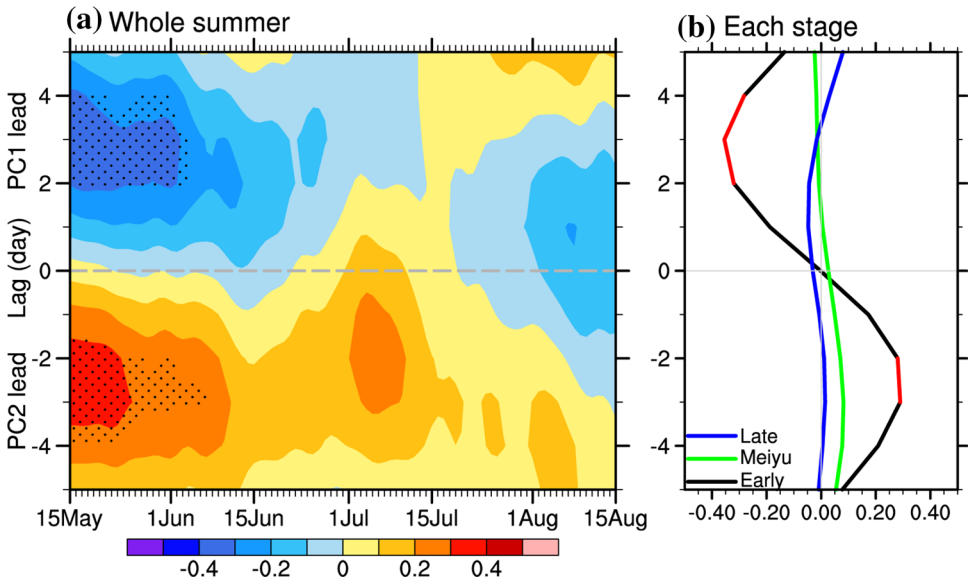

Fig. 7 Relationship between two leading modes of ISV. **a** Shown is 31-day-sliding lead-lag correlation coefficient map between PC1 and PC2 for the whole summer. Stippling denotes correlation significant at the 95% confidence level. **b** Same as **a**, except for the average of each stage. Black, green and blue lines represent the early summer, Meiyu season and late summer, respectively. Red color denotes correlation significant at the 95% confidence level

Sea at day 0, and dipole convection anomalies with wet anomaly over southeastern China and dry anomaly over the South China Sea appear on day −2 before the peak phase of UM (Fig. 8a). This dry convection anomaly over the South China Sea is weaker than the wet anomaly over southeastern China, and there is no significant preceding ISV observed over the tropics, which means that this dry convection anomaly over the South China Sea and Philippine Sea is more like a response to the divergence of wet convection anomaly over southeastern China rather than an intraseasonal oscillation originated from the western tropical Pacific.

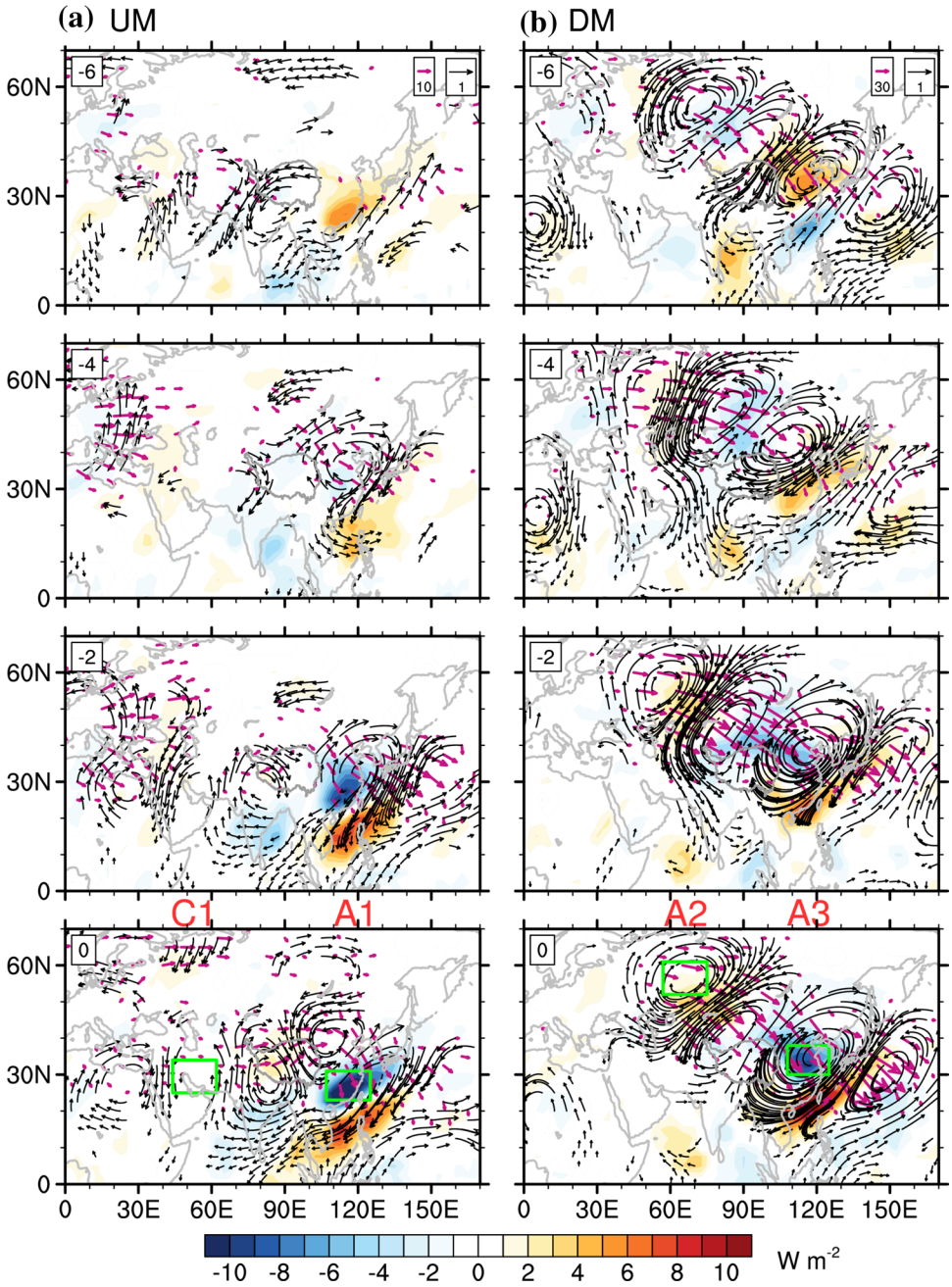

Fig. 8 Potential predictability for early summer. **a** Lagged regression maps of 8–30-day-filtered OLR (shading; W m^{-2}), 200-hPa wind (black vectors; m s^{-1}) and 200-hPa wave-activity flux (red vectors; m^2 s^{-2}) anomalies onto PC1 during early summer of 1979–2016. Only OLR, wind and wave-activity flux anomalies significant at the 95% confidence level are shown. **b** The same as **a** except for PC2. The letters A and C at day 0 indicate the anticyclone and cyclone marked by the squares, respectively

Before the peak phase of UM (Fig. 8a), however, a strong preceding mid-latitude wave train appears starting from the Mediterranean, via Central Asia, and Tibetan Plateau, toward East Asia, which has a "silk road"-like teleconnection pattern (Enomoto et al. 2003; Lu et al. 2002). At the peak phase of UM on day 0, upper-level anticyclonic anomaly over southeastern China causes upward motion and enhances the precipitation there.

Related to DM in early summer, there is also no significant preceding signal from the tropics, and the negative convection anomaly along the coastal region of southeastern China at day 0 also propagates from northeastern China at day − 6 (Fig. 8b). Strong preceding mid-latitude wave train is observed from western Siberian, via southwestern Lake Baikal and Northeast Asia, toward the WNP (Fig. 8b). At the peak phase of DM, the upper-level anticyclonic anomaly is located north of the Yangtze River, causing upward motion there, and strong negative convection anomaly is also excited over the northern South China Sea and Philippine Sea (Fig. 8b).

In early summer, the tropical signal over the South China Sea and Philippine Sea is actually originated from the southward propagation of ISV over China. These results mean that both UM and DM are mainly related

to mid-latitude wave train rather than to the tropical ISV during early summer.

5.2 Meiyu season

During the Meiyu season, UM is related to significant negative convection anomaly propagating from the western equatorial Pacific at day −6 to the South China Sea at day 0 (Fig. 9a). In the upper troposphere, there is a "Polar Eurasia" pattern-like teleconnection that has dipole height anomalies over the polar and northern China/Mongolia regions. The significant southward propagating wave train is observed from western Lake Baikal toward Northeast Asia, East Asia, and Indo-China Peninsula (Fig. 9a). At day 0, the strong upper-tropospheric cyclonic and anticyclonic anomalies sandwich southeastern China, and cause strong upper-tropospheric divergence and upward motion there. The lower-tropospheric cyclonic anomaly over southeastern China is also supported by the anticyclonic anomaly over the South China Sea and Philippine Sea.

Prior to the peak phase of DM during the Meiyu season (Fig. 9b), significant anticyclonic anomaly is also observed over the western tropical Pacific, which propagates from the Philippine Sea at day −6 to the northern South China Sea at

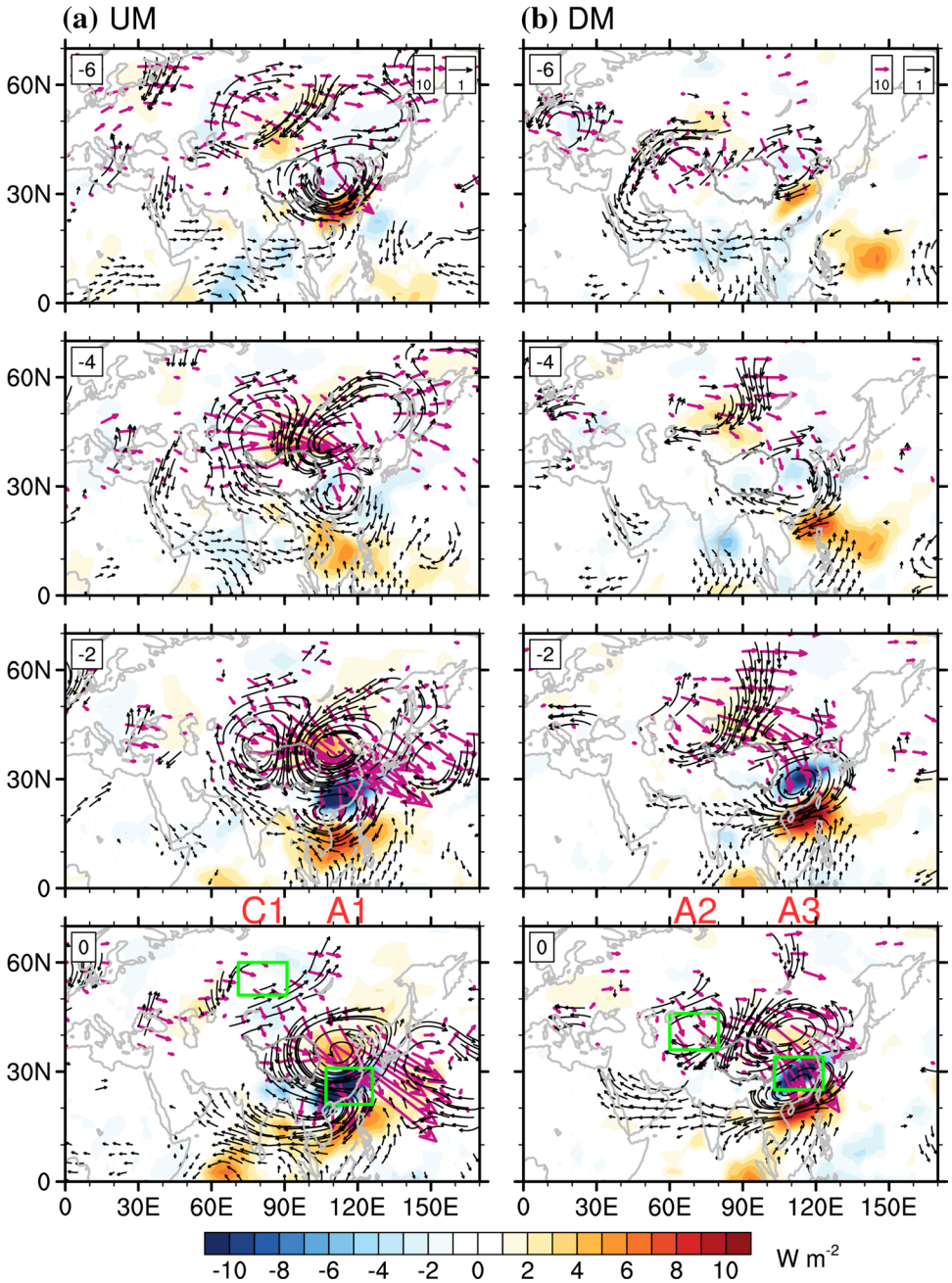

Fig. 9 Potential predictability for Meiyu season. Same as in Fig. 8, except for the Meiyu season

day 0. Significant wave train is observed from Europe, via the Caspian Sea, Mongolian Plateau and Northeast Asia, toward southeastern China. At day 0, the strong lower-troposphere anticyclonic anomaly over the northern South China Sea and upper-level westerly jet both enhance the precipitation over the mid-lower reaches of the Yangtze River. During the Meiyu season, UM and DM are related to tropical intraseasonal signal and mid-latitude wave train.

For these early summer and Meiyu season, the mid-latitude wave trains of both UM and DM exhibit a typical barotropical structure, and they turn into a baroclinic structure over East Asia where strong precipitation anomaly occurs (Fig. 10). This is consistent with the results of Fujinami and Yasunari (2009) and Yang et al. (2014).

5.3 Late summer

During late summer, UM is related to tropical westward-propagating positive convection anomaly from the Philippine Sea at day −6 to southeastern China at day 0, and this tropical cyclone-like intraseasonal signal can appear over southeastern China at day 0 and results in UM there (Fig. 11a). In the upper troposphere, a weak "silk road"-like wave train from the Mediterranean, Central Asia, Mongolian Plateau, to East Asia is also observed (Fig. 11a), while it is much weaker than that observed in early summer (Fig. 8a).

DM is also related to westward-propagating tropical cyclonic-like negative convection anomaly from the Philippine Sea at day −6 (Fig. 11b). This negative convection anomaly, however, can only land over the coastal region of southeastern China at day 0. The southwesterly to its northwest flank should bring moisture to the mid-lower reaches of the Yangtze River, resulting in DM. In the upper troposphere, a mid-latitude wave train from western Siberian, Mongolian, Northeast Asian to the WNP is observed, while strong signal mainly occurs downstream from Northeast Asia and WNP to the east of Japan (Fig. 11b).

In summary, both UM and DM are only related to preceding mid-latitude wave trains in early summer. In the Meiyu season, the tropical intraseasonal signal also contributes to the ISV of China summer precipitation in addition to the mid-latitude wave trains. In late summer, the tropical cyclone-like convection anomaly can land over whole China or coastal region of southeastern China, and the mid-latitude wave trains are relatively weaker than those in early summer and Meiyu season.

5.4 Change of mean state

To understand these different potential predictability sources for the ISV in the three stages, the mid-latitude westerly jet and monsoon trough are investigated next. They are important for mid-latitude wave train (Lee et al. 2009; Liu and Wang 2013; Straub and Kiladis 2002; Webster 1982; Webster and Chang 1988) and tropical intraseasonal signal (Wang et al. 2004, 2009).

From early summer to late summer, the upper-tropospheric westerly jet becomes weakened and shifts northward away from China's monsoon region (Fig. 12a–c), associated with the onset of Meiyu in mid-June (Li et al. 2004) and rainfall over North China in mid-July (Du et al. 2009). Since the westerly jet acts as a waveguide for the mid-latitude wave train (Lee et al. 2009; Liu and Wang 2013; Straub and Kiladis 2002; Webster 1982; Webster and Chang 1988), the mid-latitude wave train also moves northward along with the westerly jet. In late summer, the mid-latitude wave train far

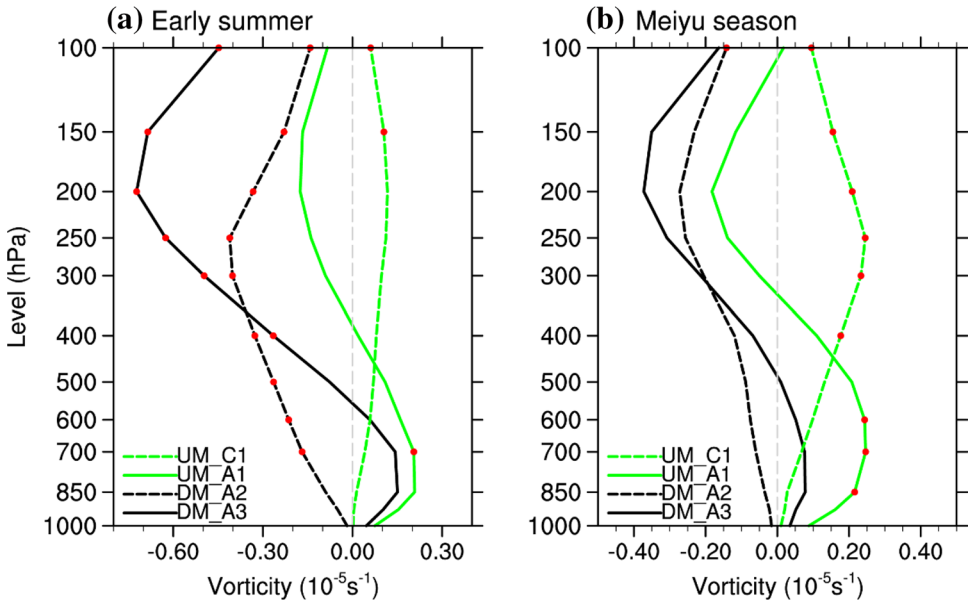

Fig. 10 Vertical structures along the wave train in different stages. Vertical profile of area-averaged regressed vorticity (10^{-5} s^{-1}) at day 0 for the selected areas in Fig. 8 for early summer (**a**) and in Fig. 9 for Meiyu season (**b**). The red dots denote regressions being significant at the 95% confidence level

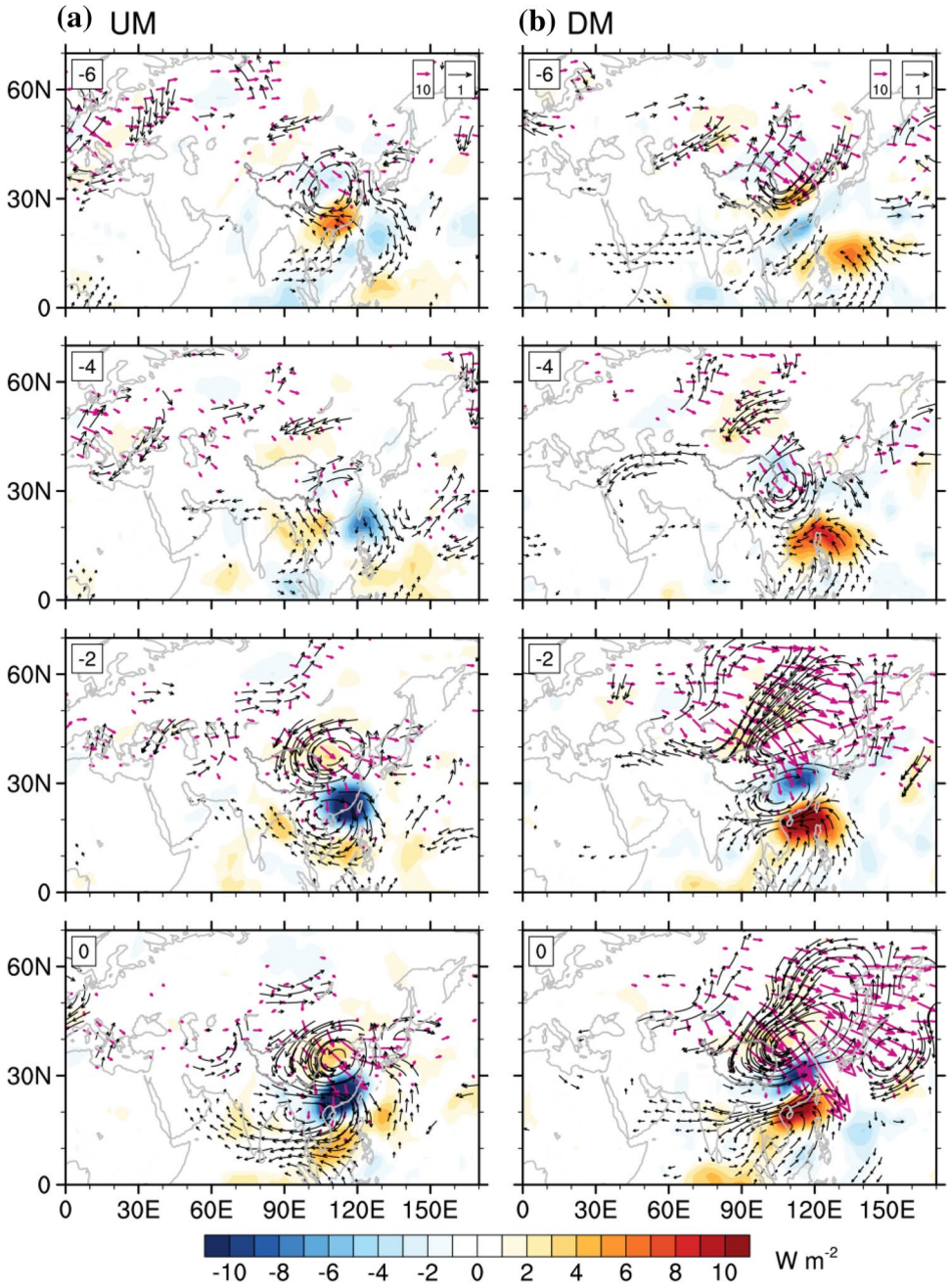

Fig. 11 Potential predictability for late summer. Same as in Fig. 8, except for late summer

away from the monsoon region should have weak effects on the ISV of China's summer precipitation (Fig. 12c).

The effects from the tropics are also mean-state-dependent. The monsoon trough, represented by the 1000–850 hPa averaged vorticity (Li and Pan 2007), is a region favoring the low-level atmospheric convergence, large moisture flux and small vertical wind shear (Lander 1994; Ritchie and Holland 1999) and favoring the generation of tropical ISV (Huang et al. 2016; Ko and Hsu 2006; Liu et al. 2016; Liu and Wang 2013). In early summer, the monsoon trough over the WNP is very weak, so the ISV cannot prevail there (Fig. 12d). In the Meiyu season and late summer, the ISV becomes strong due to the formation of monsoon trough (Fig. 12e, f), which can propagate westward to affect the ISV over China.

6 Summary and discussion

We studied seasonal evolution of dominant ISV modes of China summer precipitation. Following the seasonal evolution of monsoon precipitation, the seasonal evolution of the ISV activity can be separated to three stages: early summer stage from 1st May to 14th June, Meiyu season stage from 15th June to 15th July, and late summer stage from 16th

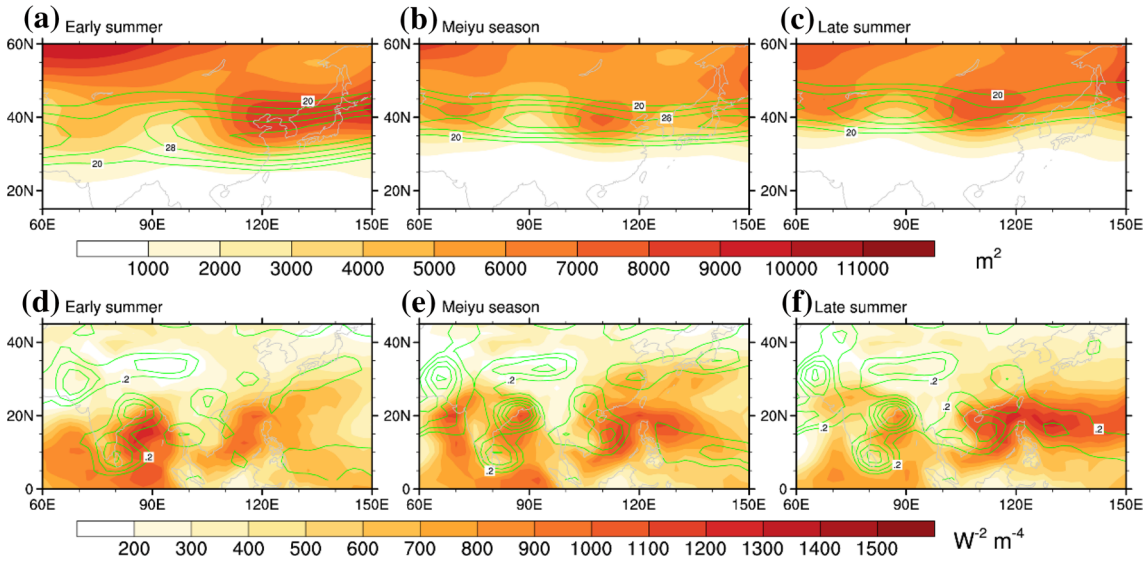

Fig. 12 Mean states during different stages. Mean 200-hPa zonal wind (contour; m s^{-1}) and variance (shading; m^2) of 8–80-day-filtered 200-hPa geopotential height anomaly for **a** early summer, **b** Meiyu season, and **c** late summer during 1979–2016. Counter interval is 4 m s^{-1}. **d**–**f** The same as **a**–**c**, except for background 1000–850 hPa averaged vorticity (contour; contour interval 0.4×10^{-5} s^{-1}) and variance (shading; W^2 m^{-4}) of 8–80-day-filtered OLR anomaly in each stage

July to 31st August. The ISV of China summer precipitation mainly prevails over southeastern China to the south of the Yangtze River in early summer, and it prevails around the mid-lower reaches of the YRB and Jianghuai region during the Meiyu season. In late summer, the maximum ISV activity retreats to the coastal region of southeastern China and eastern Tibetan Plateau. The ISV activity in the Meiyu season is stronger than those in early and late summers.

The ISV of China summer precipitation has two leading modes, represented by the UM over southeastern China to the south of the Yangtze River and by the DM between coastal region of southeastern China and mid-lower reaches of the Yangtze River. Both UM and DM are also observed in each summer stage, except that their amplitude follows the change of ISV activity in different stages. The strong precipitation anomaly over the mid-lower reaches of the Yangtze River only occurs during the Meiyu season in DM. Both UM and DM in the Meiyu season are stronger than those in early and late summers. And both UM and DM are dominated by 8–15-day oscillations in early and late summers, while they are dominated by 8–25-day oscillations during the Meiyu season. These UM and DM only compose southward propagation in early summer, while their lagged correlation is low.

As summarized in Fig. 13, both UM and DM are only related to strong preceding mid-latitude wave trains in early summer, which provides a potential predictability source, and no preceding tropical signal can be observed. During the Meiyu season, the preceding tropical intraseasonal signal from the western tropical Pacific provides another predictability source for these two leading modes of ISV, in addition to the mid-latitude wave train. In late summer, the effect of preceding mid-latitude wave train is weak. The strong tropical cyclone-like intraseasonal signal can land over southeastern China to form the UM and over the coastal region of southeastern China to form the DM. Changes of these potential predictability sources in different stages are attributed to the changes of mean states. The weak ISV over the WNP in early summer before the formation of monsoon trough will limit the effect of tropical signal on the ISV of China summer monsoon, while the northward shift of upper-tropospheric westerly jet in late summer prohibits the effect of mid-latitude wave train. Only in the Meiyu season, these tropical and extratropical signals work together to affect the ISV of China summer precipitation.

Due to advance of the EASM, significant seasonal evolution in ISV of China summer precipitation and its associated preceding tropical and mid-latitude signals challenge our prediction system. The new empirical prediction system should have different weights in different summer stages to capture this seasonal evolution, as considered in the subseasonal prediction system with machine learning over Western United States (Hwang et al. 2019).

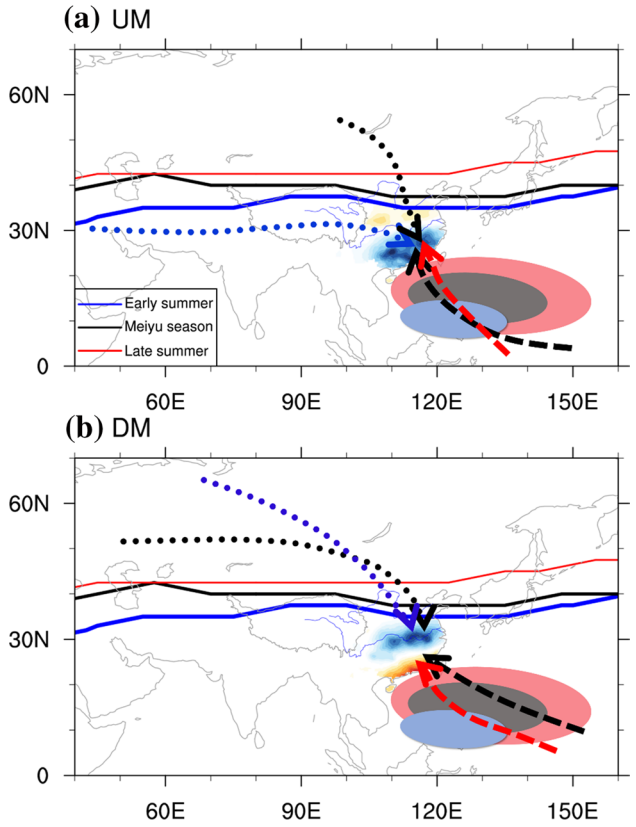

Fig. 13 Schematic diagram for two major ISV modes in different stages. **a** Propagation of mid-latitude wave trains (dotted line with arrowhead) and tropical ISV (dashed line with arrowhead) related to the ISV precipitation (shading) in UM for early summer (blue), Meiyu season (black), and late summer (red). The lines and ellipses denote the upper-level westerly jet and monsoon trough, respectively. The strength of westerly jet and monsoon trough is proportional to the line width and ellipse radius, respectively. **b** The same as **a,** except for the DM

Acknowledgements This work was supported by the National Key R&D Program of China (2018YFA0606203) and the Natural Science Foundation of China (41420104002), and by the Natural Science Foundation of Jiangsu Province (BK20150907 and 14KJA170002).

References

Cao X, Ren X, Yang X, Fang J (2012) The quasi-biweekly oscillation characteristics of persistent severe rain and its general circulation anomaly over southeast China from May to August. Acta Meteorol Sin 70:766–778

Chen GT (2004) Research on the phenomena of Meiyu during the past quarter century: an overview. In: The East Asian Monsoon. World Scientific, Singapore

Chen L, Zhu C (2001) Analysis of the characteristics of 30–60 day low-frequency oscillation over Asia during 1998 SCSMEX. Adv Atmos Sci 18:623–638

Chen L, Zhang B, Zhang Y (2006) Progress in research on the East Asian monsoon. J Appl Meteorol Sci 17:711–724

Ding Y (2004) Seasonal March of the East Asian summer monsoon. In: The East Asian monsoon. World Scientific Publisher, Singapore

Ding Y, Chan JCL (2005) The East Asian summer monsoon: an overview. Meteorol Atmos Phys 89:117–142

Ding Y-H, Wang Z-Y (2008) A study of rainy seasons in China. Meteorol Atmos Phys 100:121–138

Du Y, Zhang Y, Xie Z (2009) Location variation of the East Asia subtropical westerly jet and its effect on the summer precipitation anomaly over Eastern China. Chin J Atmos Sci 33:581–592

Duchon CE (1979) Lanczos filtering in one and two dimensions. J Appl Meteorol 18:1016–1022

Enomoto T, Hoskins BJ, Matsuda Y (2003) The formation mechanism of the Bonin high in August. Q J R Meteorol Soc 129:157–178

Fujinami H, Yasunari T (2009) The effects of midlatitude waves over and around the Tibetan Plateau on submonthly variability of the East Asian summer monsoon. Mon Weather Rev 137:2286–2304

Gao M-N, Yang J, Wang B, Zhou S-Y, Gong D-Y, Kim SJ (2017) How are heat waves over Yangtze River valley associated with atmospheric quasi-biweekly oscillation? Clim Dyn. https://doi.org/10.1007/s00382-017-3526-z

Hsu PC, Lee JY, Ha KJ (2016) Influence of boreal summer intraseasonal oscillation on rainfall extremes in southern China. Int J Climatol 36:1403–1412

Huang F, Huang S, Zhang X (2008) Study on the climatological intraseasonal oscillation of Chinese rainfall. Period Ocean Univ China 38:173–177

Huang R, Huangfu J, Liu Y, Feng T, Wu L, Chen J, Wang L (2016) Progress in recent research on the processes and physical mechanisms involved in the influence of the western Pacific warm pool on the monsoon trough and tropical cyclone activity over the western North Pacific. Chin J Atmos Sci 40:877–896

Hutchinson MF (1995) Interpolating mean rainfall using thin plate smoothing splines. Int J Geogr Inf Syst 9:385–403. https://doi.org/10.1080/02693799508902045

Hwang J, Orenstein P, Cohen J, Pfeiffer K, Mackey L (2019) Improving subseasonal forecasting in the western U.S. with machine learning. In: The 25th ACM SIGKDD conference on knowledge discovery and data mining (KDD'19), August 4–8, 2019, Anchorage. ACM, New York. https://doi.org/10.1145/3292500.3330674

Kalnay E et al (1996) The NCEP/NCAR 40-year reanalysis project. Bull Am Meteorol Soc 77:437–472

Kikuchi K, Wang B, Kajikawa Y (2011) Bimodal representation of the tropical intraseasonal oscillation. Clim Dyn 38:1–12

Ko K, Hsu H (2006) Sub-monthly circulation features associated with tropical cyclone tracks over the East Asian monsoon area during July–August season. J Meteorol Soc Jpn 84:871–889

Lander MA (1994) An exploratory analysis of the relationship between tropical storm formation in the Western North Pacific and ENSO. Mon Weather Rev 122:333–360

Lau WKM, Waliser DDE (2005) Intraseasonal variability in the atmosphere–ocean climate system. Springer, Berlin

Lee S-K, Wang C, Mapes BE (2009) A simple atmospheric model of the local and teleconnection responses to tropical heating anomalies. J Clim 22:272–284

Lee J et al (2013) Real-time multivariate indices for the boreal summer intraseasonal oscillation over the Asian summer monsoon region. Clim Dyn 40:493–509

Li C-Y, Pan J (2007) The interannual variation of the South China sea summer monsoon trough and its impact. Chin J Atmos Sci 31:1049–1058

Li C, Wang J, Lin S, Cho H (2004) The relationship between East Asian summer monsoon activity and northward jump of the upper westerly jet location. J Atmos Sci 28:641–658

Liang P, Ding Y-H (2012) Climatologic characteristics of the intraseasonal oscillation of East Asian meiyu. Acta Meteorol Sin 70:418–435
Liebmann B, Smith CA (1996) Description of a complete (interpolated) outgoing longwave radiation dataset. Bull Am Meteorol Soc 77:1275–1277
Liu F, Wang B (2013) Mechanisms of global teleconnections associated with the Asian summer monsoon: an intermediate model analysis. J Clim 26:1791–1806
Liu F, Li T, Wang H, Deng L, Zhang Y (2016) Modulation of boreal summer intraseasonal oscillations over the Western North Pacific by ENSO. J Clim 29:7189–7201
Livezey RE, Chen WY (1983) Statistical field significance and its determination by Monte Carlo techniques. Mon Weather Rev 111:46–59
Lu RY, Oh JH, Kim BJ (2002) A teleconnection pattern in upper-level meridional wind over the North African and Eurasian continent in summer. Tellus A 54:44–55
Mao J, Chan JCL (2005) Intraseasonal variability of the South China Sea summer monsoon. J Clim 18:2388–2402
New M, Hulme M, Jones P (2000) Representing twentieth-century space-time climate variability. Part I: development of a 1961–90 mean monthly terrestrial climatology. J Clim 12:829–856
North GR, Bell TL, Cahalan RF, Moeng FJ (1982) Sampling errors in the estimation of empirical orthogonal functions. Mon Weather Rev 110:699–706. https://doi.org/10.1175/1520-0493(1982)110%3c0699:seiteo%3e2.0.co;2
Ren P-f, Ren H-L, Fu J-X, Wu J, Du L (2018) Impact of boreal summer intraseasonal oscillation on rainfall extremes in Southeastern China and its predictability in CFSv2. J Geophys Res Atmos 123:4423–4442. https://doi.org/10.1029/2017jd028043
Ritchie EA, Holland GJ (1999) Large-scale patterns associated with tropical cyclogenesis in the Western Pacific. Mon Weather Rev 127:2027–2043
Shepard DS (1984) Computer mapping: the SYMAP interpolation algorithm. Spat Stat Models 40:133–145
Son JH, Seo KH, Wang B (2019) Dynamical control of the Tibetan Plateau on the East Asian summer monsoon. Geophys Res Lett 46:7672–7679. https://doi.org/10.1029/2019gl083104
Stan C, Straus DM, Frederiksen JS, Hai L, Schumacher C (2017) Review of tropical–extratropical teleconnections on intraseasonal time scales. Rev Geophys 55:902–937
Straub KH, Kiladis GN (2002) Observations of a convectively coupled Kelvin wave in the Eastern Pacific ITCZ. J Atmos Sci 59:30–53
Takaya K, Nakamura H (2001) A formulation of a phase-independent wave-activity flux for stationary and migratory quasigeostrophic eddies on a zonally varying basic flow. J Atmos Sci 58:608–627
Tao SY, Chen LX (1987) A review of recent research on the East Asian summer monsoon. In: Chang C-P, Krishnamurti TN (eds) China monsoon meteorology. Oxford University Press, Oxford, pp 60–92
Vitart F et al (2017) The subseasonal to seasonal (S2S) prediction project database. Bull Am Meteorol Soc 98:163–173. https://doi.org/10.1175/bams-d-16-0017.1
Wang B (2006) The Asian monsoon. Springer, Berlin
Wang B, LinHo (2002) Rainy season of the Asian-Pacific summer monsoon. J Clim 15:386–398
Wang B, Xu X-H (1997) Northern hemisphere summer monsoon singularities and climatological intraseasonal oscillation. J Clim 10:1071–1085
Wang B, LinHo Zhang YS, Lu MM (2004) Definition of South China Sea monsoon onset and commencement of the East Asian summer monsoon. J Clim 17:699–710
Wang B, Huang F, Wu Z, Yang J, Fu X, Kikuchi K (2009) Multi-scale climate variability of the South China Sea monsoon: a review. Dyn Atmos Oceans 47:15–37
Wang X, Chen G, Huang R (2015) Different characteristics of the quasi-biweekly oscillation over the South China Sea in two boreal summer stages. Theor Appl Climatol 126:1–13
Wang M, Wang J, Duan A, Liu Y, Zhou S (2018) Coupling of the quasi-biweekly oscillation of the Tibetan Plateau summer monsoon with the arctic oscillation. Geophys Res Lett 45:7756–7764. https://doi.org/10.1029/2018gl077136
Webster PJ (1982) Cross-equatorial response to middle-latitude forcing in a zonally varying basic state. J Atmos Sci 39:722–733
Webster PJ, Chang HR (1988) Equatorial energy accumulation and emanation regions: impacts of a zonally varying basic state. J Atmos Sci 45:803–829
Wei L, Fang J, Yang X (2017) Low frequency oscillation characteristics of 12–30d persistent heavy rainfall over South China. Acta Meteorol Sin 75:80–97
Wheeler MC, Hendon HH (2004) An all-season real-time multivariate MJO index: development of an index for monitoring and prediction. Mon Weather Rev 132:1917–1932
Wu J, Gao X (2013) A gridded daily observation dataset over China region and comparison with the other datasets. Chin J Geophys 56:1102–1111
Wu R, Wang B (2001) Multi-stage onset of the summer monsoon over the western North Pacific. Clim Dyn 17:277–289
Xie P-P, Yatagai A, Chen M-Y, Hayasaka T, Fukushima Y, Liu C-M, Yang S (2007) A gauge-based analysis of daily precipitation over East Asia. J Hydrometeorol 8:607
Xu Y, Gao X, Shen Y, Xu C, Shi Y, Giorgi F (2009) A daily temperature dataset over china and its application in validating a RCM simulation. Adv Atmos Sci 26:763–772
Yang S, Li T (2016) Intraseasonal variability of air temperature over the mid-high latitude Eurasia in boreal winter. Clim Dyn 47:2155–2175
Yang J, Wang B, Bao Q (2010) Biweekly and 21–30-day variations of the subtropical summer monsoon rainfall over the lower reach of the Yangtze River Basin. J Clim 23:1146–1159
Yang J, Bao Q, Wang B, Gong DY, He H, Gao MN (2014) Distinct quasi-biweekly features of the subtropical East Asian monsoon during early and late summers. Clim Dyn 42:1469–1486
Yang J, Bao Q, Wang B, He H-Z, Gao M-N, Gong D-Y (2017) Characterizing two types of transient intraseasonal oscillations in the Eastern Tibetan Plateau summer rainfall. Clim Dyn 48:1749–1768
Zhang Y-L, Li B-Y, Zheng D (2002) A discussion on the boundary and area of the Tibetan Plateau in China. Geogr Res 21:1–8
Zhu Q, Xu G (2000) The features of low frequency precipitation in South China with South China Sea low frequency summer monsoon activity in the summer of 1998. Sci Meteorol Sin 20:239–248